

REVIEW

The physics of small megavoltage photon beam dosimetry ^{*†}

Pedro Andreo

*Department of Medical Radiation Physics and Nuclear Medicine, Karolinska University Hospital, and Department of Oncology-Pathology, Karolinska Institutet
SE-171 76 Stockholm, Sweden*

16 October 2017

Abstract

The increased interest during recent years in the use of small megavoltage photon beams in advanced radiotherapy techniques has led to the development of dosimetry recommendations by different national and international organizations. Their requirement of data suitable for the different clinical options available, regarding treatment units and dosimetry equipment, has generated a considerable amount of research by the scientific community during the last decade. The multiple publications in the field have led not only to the availability of new invaluable data, but have also contributed substantially to an improved understanding of the physics of their dosimetry. This work provides an overview of the most important aspects that govern the physics of small megavoltage photon beam dosimetry.

Keywords: small fields dosimetry; detector material; detector design; dosimetry protocols

^{*}Based on a Teaching lecture at the *International Conference on Advances in Radiation Oncology (ICARO2)*, International Atomic Energy Agency (IAEA), Vienna 20-23 June 2017

[†]Preprint of the article published in *Radiotherapy and Oncology* 126 (2018) 205-213. The journal policy is that a published article can not have more than six figures, the rest is available in electronic form as "Supplementary data" at <https://doi.org/10.1016/j.radonc.2017.11.001>. This preprint includes all the figures (in colour, when available) according to their use in the text, providing a consistent flow of the manuscript.

1 Introduction

Radiation therapy with small photon beams can be considered to have its roots in an old technique pioneered in the early fifties by the Swedish neurosurgeon Leksell for the stereotactic radiosurgery (SRS) of small brain tumours and malformations [1]; it led to the subsequent development of the ^{60}Co -based Gamma Knife[®] [2]. The use of clinical accelerators for radiosurgery emerged almost simultaneously in the UK and USA. Both type of treatment units, ^{60}Co -based and linacs, soon became used worldwide. Although initially SRS was used as a surgery procedure, stereotactic techniques were extended rapidly to cancer radiotherapy treatments (SRT), not only for the brain but also for stereotactic body radiation therapy (SBRT). The recent ICRU Report 91 on stereotactic treatments with small photon beams [3] includes a detailed summary of the history of SRS and SRT.

Further developments in radiotherapy techniques have led to a proliferation of the use of small fields, paralleled with the development of specialized dedicated treatment units like the TomoTherapy[®], CyberKnife[®] or new Gamma Knife[®] models. Unfortunate accidents have occurred, however, in some radiotherapy centres [4, 5] that in most cases were related to the inappropriate use of dosimetry procedures and instrumentation intended for conventional radiotherapy dosimetry.

The last decade has witnessed a substantial interest in the development of dosimetry recommendations for small photon beams, a task led by a comprehensive IPEM report [6] and followed by other organizations. Among them was a joint IAEA-AAPM project initiated in 2007 that has culminated with the publication of the international Code of Practice IAEA TRS-483 [7]. Its development included the early publication of a new dosimetry formalism for small and non-standard fields [8] that has triggered considerable research by the scientific community (see e.g. refs. [9, 10, 11, 12, 13, 14, 15, 16, 17, 18, 19, 20, 21, 22, 23, 24, 25, 26, 27, 28, 29, 30, 31, 32, 33, 34, 35, 36, 37, 38, 39, 40, 41, 42, 43, 44, 45]; additional references can be found in [7]). The large number of publications in the field has led not only to the availability of different sets of new data for combinations of machine and detector types, but has also contributed substantially to the enhancement of our understanding of the physics of small megavoltage photon beam dosimetry, which is the task of the present review.

2 When is a photon beam small?

There are three general conditions to consider if a photon beam can be classified as small, and at least one of them must be fulfilled:

- (i) There is a loss of lateral charged-particle equilibrium in a region of interest, usually around the beam central axis, where a detector volume is positioned for reference and relative dosimetry.
- (ii) There is a partial occlusion of the primary photon source by the beam collimating system, which is a machine-specific issue.
- (iii) There is a mismatch between the detector cross-sectional size and the field size at the depth of measurement, and perturbation effects much larger than in the case of conventional broad radiotherapy beams.

These conditions and the reasons for their incidence are discussed in detail in the following sections.

3 Loss of lateral charged-particle equilibrium

Loss of lateral charged-particle equilibrium (LCPE) is a fundamental condition applicable to a general photon radiation field that is narrow in its lateral extension. It occurs in photon beams when the beam half-width or radius is smaller than the maximum lateral range of secondary electrons. Lack of LCPE

is problematic for dosimetry since the balance of charged particles laterally scattered in and out of the beam cannot be achieved; for example, in the presence of a cavity with a density higher than that of the medium (usually water) more particles are scattered outwards than inwards.

Based on the pioneer work of Li *et al.* [46], the ratio of absorbed dose to collision kerma, D/K_{col} , is used as a measure of the degree of charged-particle equilibrium (CPE), or rather, transient charged-particle equilibrium (TCPE), see Fig. 1. The minimum beam radius for which $D/K_{\text{col}} = 1$ defines what is termed *lateral charged-particle equilibrium range*, denoted by r_{LCPE} .

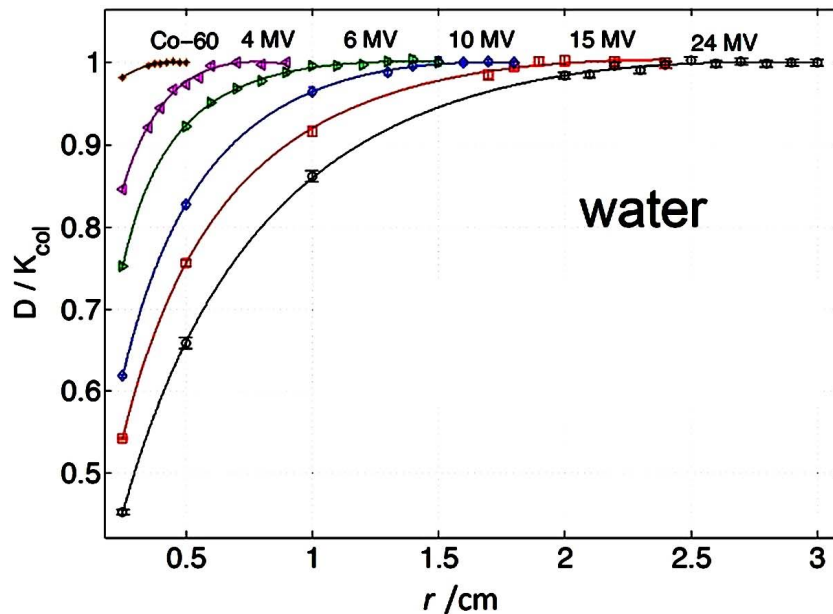


Figure 1: Monte Carlo calculated D/K_{col} ratios in water at 5 cm depth on the central axis of photon beams of different nominal energy, as a function of the radius of the beam. The ratios are normalized to the values corresponding to broad beam transient charged-particle equilibrium (TCPE) conditions. The lateral charged-particle equilibrium range r_{LCPE} is determined as the field radius for which $D/K_{\text{col}} = 1$. From Papaconstadopoulos (2016) [47]. Reproduced with permission.

Expressed as a function of the photon beam quality specifier $\text{TPR}_{20,10}$ for the common reference field size of $10 \text{ cm} \times 10 \text{ cm}$, the lateral charged-particle equilibrium range is given in IAEA TRS-483 by

$$r_{\text{LCPE}} [\text{cm}] = 8.369 \cdot \text{TPR}_{20,10} - 4.382 \quad (1)$$

where the coefficients were obtained from a fit to the new Monte Carlo data calculated by Papaconstadopoulos [47] shown in Fig. 1.

The intrinsic practical condition for a small beam is that, for measurements in a given beam quality, the distance from the detector *outer boundary* to the radiation field edge is smaller than r_{LCPE} . Note that this condition includes detector components surrounding the radiation sensitive volume (RSV), as they contribute substantially to the response of a detector.

4 Partial source occlusion

In practice, for small megavoltage beams produced by clinical accelerators, the necessary collimation to reduce the field size produces a partial occlusion of the primary radiation source and a relative increase

of the penumbra, both effects being related to the size of the radiation source, i.e., the “spot size” of the electrons impinging on the target where photons are produced by bremsstrahlung interactions. Figure 2 illustrates the partial source occlusion and penumbra overlap in a narrow photon beam compared with the situation in a broad beam.

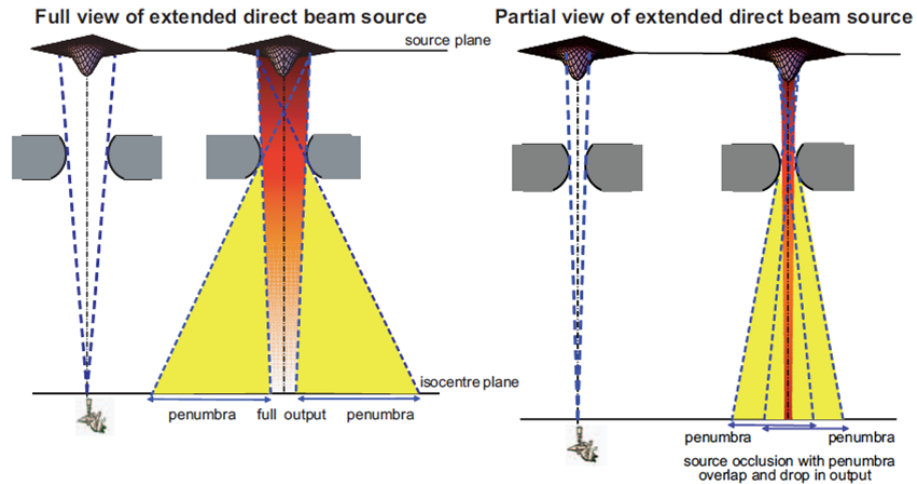


Figure 2: Schematic illustration of the direct beam source occlusion effect and penumbra overlap in a narrow photon beam (right panel), which does not occur in broad beams (left panel). From IPEM Report 103 [6]. Copyright Institute of Physics and Engineering in Medicine 2010. Reproduced with permission.

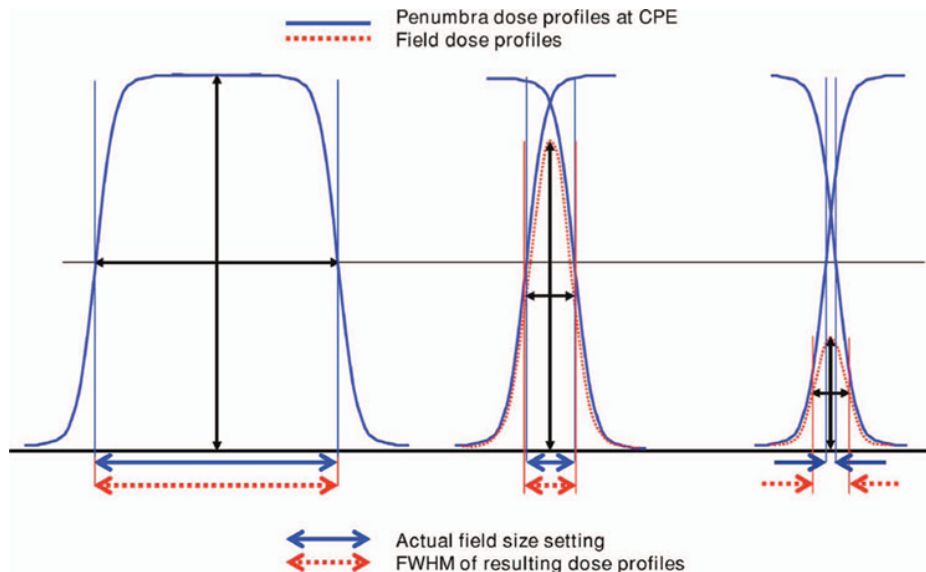


Figure 3: Effect of overlapping penumbrae on the full width at half maximum (FWHM) of the lateral beam profile for small fields at a depth where TCPE exists, illustrating the apparent field widening compared to the collimator settings (arrows) and decreased output (height of the red dotted beam profile). From Das *et al.* (2008) [9]. Copyright John Wiley & Sons Inc. Reproduced with permission.

The consequences of the overlapping penumbrae are that, contrary to the case of large beams, in small beams the size determined by the full width at half maximum (FWHM) of a dose profile at a typical depth of 10 cm, normalized to the beam central axis, usually does not coincide with the indication of the machine collimators, that is, there is an apparent widening of the field. Of special importance is that the machine output becomes decreased. This is illustrated in Fig. 3, where the height of the resulting dose profiles decreases when the field size is reduced.

The results of partial source occlusion can then be summarized as:

- (i) Overlap of the penumbra, which is related to the machine spot (source) size
- (ii) Reduction of the relative central-axis dose, which decreases the machine output
- (iii) Apparent field widening, which causes a mismatch between the FWHM (true field size) and the collimator setting (nominal field size)

These are issues having a potential impact on the data required for radiotherapy treatment planning systems, where often the size of the beam is defined by the machine collimation system, that is, by the nominal field size.

5 Other aspects of decreasing the field size

As a result of decreasing the field size, there are two important aspects to consider in the dosimetry of small photon fields. These are the hardening of the energy spectrum, and its influence on the water-to-air stopping-power ratios for ionization chamber reference dosimetry.

It is clear that, compared with a broad beam, decreasing the field size by collimation reduces the scatter occurring in the components of the machine treatment head. Additionally, the amount of scatter occurring in the phantom also decreases, as the irradiated volume is smaller. The result is a *filtration* of the low photon energies that yields an increase in the mean energy of the respective spectra. Figure 4 illustrates the change in photon spectra in a small volume of water when the size of a 6 MV beam is decreased, showing a considerable filtration of the low-energy component that results in a substantial increase of the mean photon energy. Monte Carlo calculations for machine-specific photon beams showing the filtration and change in mean energy of photon and electron spectra have been described in ref. [48].

The practically negligible field size (and depth) dependence of the water/air stopping-power ratio is known since years [49]. Figure 5 shows the variation of $s_{w,air}$ in a 6 MV photon beam, where it can be seen that at the common reference depth of 10 cm in water, the difference in $s_{w,air}$ between the field sizes of 10 cm \times 10 cm and 0.5 cm \times 0.5 cm is only of about 0.3 %. This is a very remarkable property, confirmed more recently by other authors (see, e.g., refs. [48, 50]), because $s_{w,air}$ is one of the most important quantities in the reference dosimetry of photon beams, usually performed with an air-filled ionization chamber. It is worth mentioning that the difference in $s_{w,air}$ for conventional broad beams and for flattening filter free (FFF) beams is also of this order ($\lesssim 0.5$ %) for beam qualities around 6 MV (see ref. [7] and references therein). However, as will be shown below, in small photon beams the advantage of the constancy of $s_{w,air}$ with field size is superseded in many instances by the influence of ionization chamber perturbation effects.

6 Detector-related issues

In addition to the constraints posed by the intrinsic radiation field size and beam collimation, there are two important issues related to the properties of the detector used for the dosimetry of small photon beams. These are the detector size, relative to the dimensions of the field, and the perturbation effects caused by the detector material and its design, both playing a fundamental role in the detector response.

6.1 Detector size *versus* field size

For years, ionization chambers have been the “backbone” of radiotherapy dosimetry for conventional (broad) beams. It is well-known, on the other hand, that ion chambers are not suitable in regions with

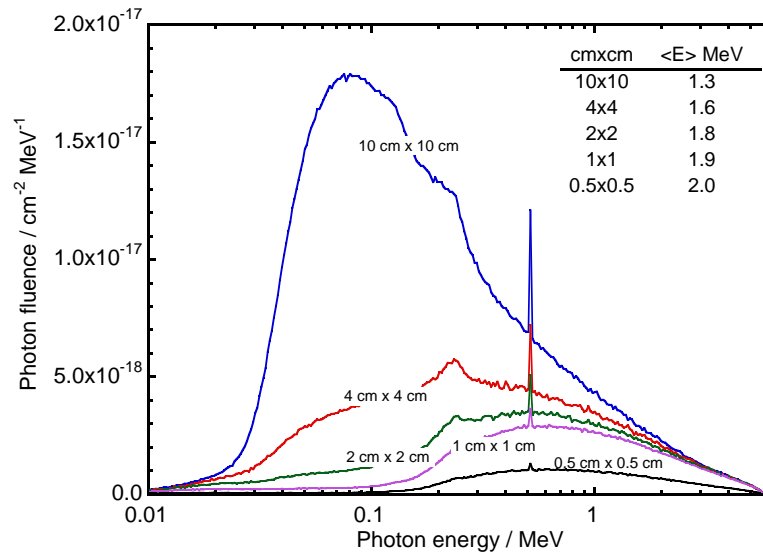


Figure 4: 6 MV photon spectra in a small water volume for different field sizes at 10 cm depth. The variation of mean photon energy with field size is from 1.3 MeV (10 cm \times 10 cm) to 2.0 MeV (0.5 cm \times 0.5 cm). Note the photon peak at 511 keV resulting from positron annihilation. Adapted from Benmakhlouf *et al.* (2014) [24]. Copyright John Wiley & Sons Inc. Reproduced with permission.

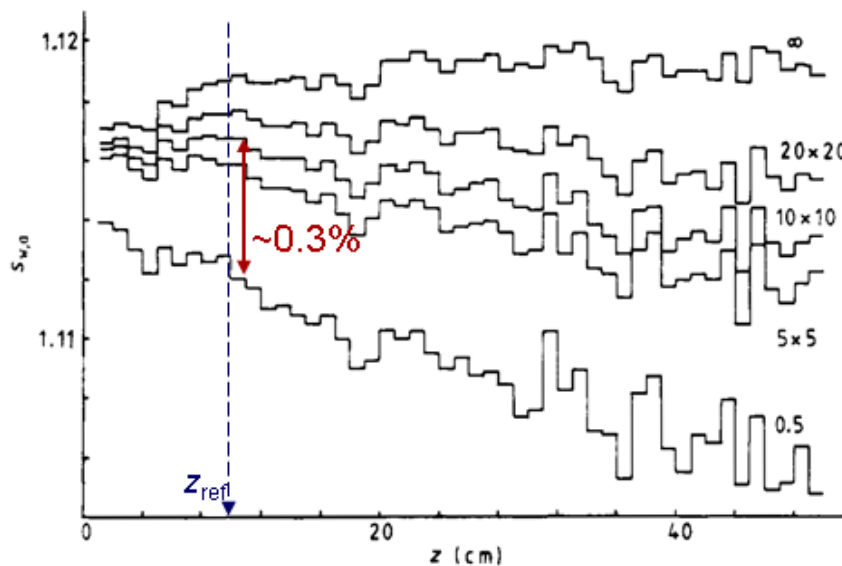


Figure 5: Field size and depth dependence of the water/air stopping-power ratio, $s_{w,air}$, in a 6 MV photon beam. From Andreo and Brahme (1986) [49]. Copyright Institute of Physics and Engineering in Medicine. Reproduced by permission of IOP Publishing. All rights reserved.

high-dose gradients or in non-uniform beams, that there are constraints regarding their size *versus* sensitivity (signal-to-noise ratio, s/n), and that their use in reference dosimetry requires relatively small fluence perturbation corrections.

An aspect that in general has not been necessary to consider in broad beams is that a region of uniform fluence is required around the chamber. This, however, becomes an important issue in small beams when the chamber size is comparable to the field dimensions or when the fluence over the chamber is not uniform, a situation illustrated in Fig. 6. Recall that, in a measurement, any detector delivers a signal averaged over its volume, which is proportional to the energy deposited in the radiation sensitive volume due to the particle fluence crossing the detector; this is called the *volume-averaging effect*. If the field

size is smaller than the chamber dimensions and particles cross only a fraction of the sensitive volume, or if the fluence over the detector is not uniform, as it occurs e.g. in broad FFF beams, the detector signal averaged over its volume will be clearly incorrect.

A chamber reading will thus depend on the ratio chamber/field-size, and the volume-averaging effect must be corrected for in order to obtain an accurate mean estimate. The required correction factor can be derived by integrating the beam dose profile at the measurement depth in water over the detector surface perpendicular to the beam direction, a modification introduced by IAEA TRS-483 to the expression originally proposed by Kawachi *et al.* [51] that did not consider the detector profile.

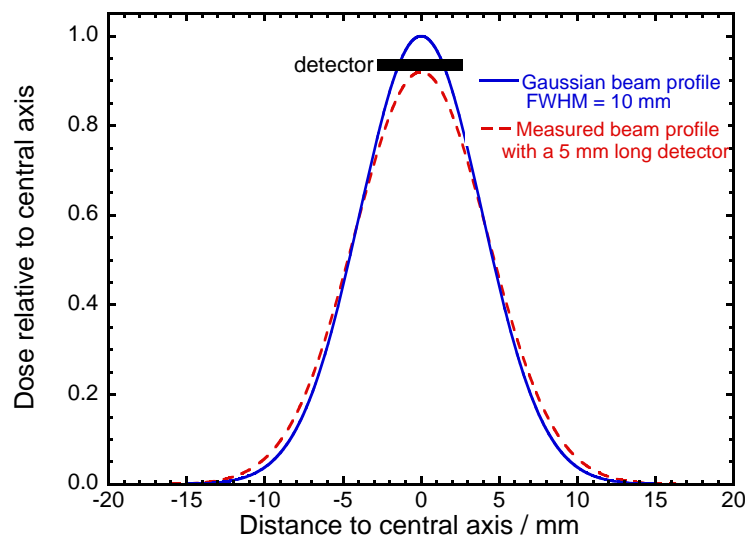


Figure 6: Illustration of the volume averaging effect. The solid blue curve is a hypothetical Gaussian beam profile having a FWHM of 10 mm; the dashed red curve represents the averaged profile that would be measured with a 5 mm long detector. Adapted from Wuerfel (2013) [22].

6.2 Detector perturbation effects

Is also well-known that reference ion chamber dosimetry is based on the Bragg-Gray principle, and this requires the use of correction factors to account for the fluence perturbation introduced by the presence of the chamber (its air-filled volume, walls, electrode, etc.) in a homogeneous medium, i.e.

$$D_{w,Q}(z_{\text{ref}}) = D_{\text{air},Q}(z_{\text{ref}}) s_{w,\text{air}} p_{\text{ch},Q} \quad (2)$$

where $p_{\text{ch},Q}$ is an overall perturbation correction factor, obtained from the product of *small* and *independent* perturbation factors, p_{ch_i} , which account for the influence of the different chamber components at the beam quality Q .

In broad photon beams, perturbation correction factors for most commercial chambers amount only to a few percent, as can be observed in Fig. 7. For $\text{TPR}_{20,10}$ values between 0.65 and 0.70, corresponding approximately to 6–10 MV, the range of perturbation factors for more than 50 ionization chambers is within less than about 2 % except for two or three outliers.

In small photon beams, perturbation correction factors can be much larger, as shown in Fig. 8 for a common PinPoint PTW chamber having a steel electrode. The figure illustrates the off-axis variation of different perturbation factors, which at the central axis, where the reference absorbed dose is determined, shows individual contributions of around 5–6 % for the displacement effect, p_{dis} , and for the partial-volume averaging effect, p_{vol} ; the combination of all contributions yields an overall perturbation

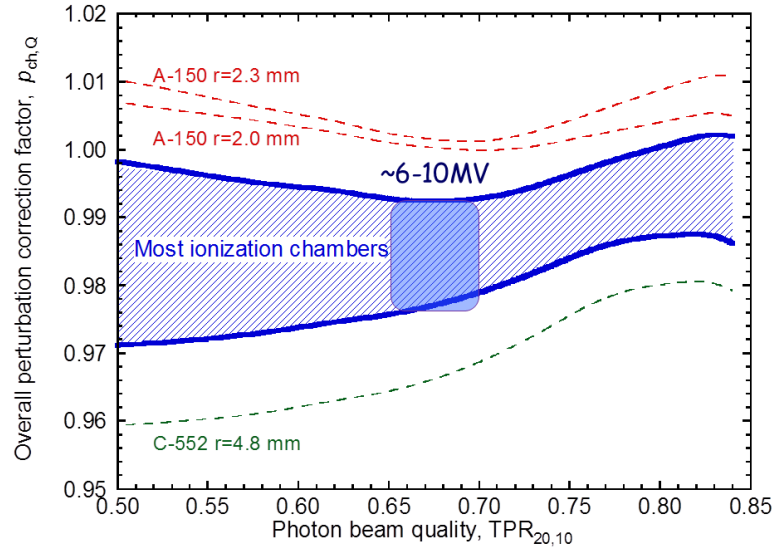


Figure 7: Average values of the overall perturbation correction factor, $p_{ch,Q}$, for megavoltage photon beams, for more than 50 ionization chamber types, as a function of the photon beam quality $TPR_{20,10}$. The range corresponding approximately to 6–10 MV is enclosed in the dark square. From *Andreo et al. (2017) [52]*. Copyright Wiley-VCH Verlag GmbH & Co KGaA. Reproduced with permission.

correction factor $p_{ch,Q}$ close to 10 %. These are too large corrections to be considered “small”, as will be discussed below.

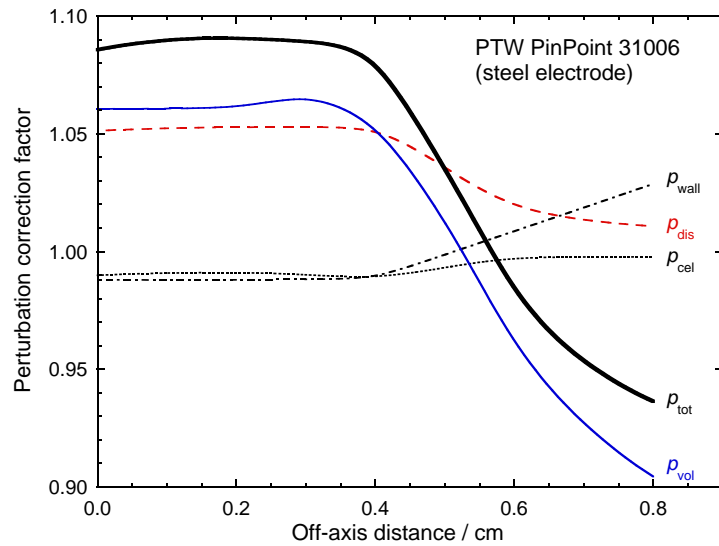


Figure 8: Monte Carlo-calculated perturbation correction factors for an ionization chamber PTW PinPoint 31006 in a $0.8 \text{ cm} \times 0.8 \text{ cm}$ beam. The curve labelled p_{tot} corresponds to the overall perturbation correction factor. From *Andreo et al. (2017) [52]* using data from *Crop et al. (2009) [10]*. Copyright Wiley-VCH Verlag GmbH & Co KGaA. Reproduced with permission.

One can then summarize the main issues related to ionization chambers in small fields by stating that volume averaging is critical for ion chamber dosimetry and that perturbations might require a considerable correction factor. The need for a volume averaging correction can be minimized using a small chamber size while keeping the chamber-to-field edge distance larger than r_{LCPE} . It should be noted that current

Monte Carlo-calculated overall perturbation factors already include volume averaging effects.

To conclude this section we will comment briefly on the role of solid-state detectors (silicon diodes, natural and synthetic CVD – chemical vapour deposition – diamonds, plastic scintillators, MOSFETs, etc.). The rationale for the interest on these detectors is mainly their mass density, much higher than that of the air in ionization chambers, which allows small detector volumes while yielding high s/n ratios; this enables high spatial resolution while partial volume effects are minimized. Solid-state detectors overcome some of the constraints in the use of small chambers (e.g., s/n ratio, corrections for polarity, stem effects, leakage, etc.) and their use for relative dosimetry has increased in recent years, being in many instances preferable to small ionization chambers. There are, however, certain issues that arise in relation to their intrinsic detector material and design, which for the smallest field sizes sometimes require considerable corrections.

7 Perturbation factors and Cavity Theory

Strictly, dosimetry based on Monte Carlo calculations does not require CPE, but most of the current formulations for converting D_{det} into D_{med} rely on CPE-based approximations. For example, the conventional stopping-power ratio medium-to-detector, $s_{\text{med,det}}$, uses the approximation of constant electron fluences, $\Phi_{\text{med}} \approx \Phi_{\text{det}}$, and departures from this approximation are taken into account with the use of perturbation factors.

As already emphasized, Bragg-Gray and other cavity theories assume small and independent detector perturbation correction factors $p_{\text{det},i}$. However, as we have seen in previous sections, for many detectors often there is no CPE in small MV fields, correction factors can be large (up to 10%) and some of the perturbation effects might be strongly correlated. This means that some of the basic common assumptions in relation to the use of cavity theories are no longer valid. One can speak of a *breakdown* of Bragg-Gray cavity theory. The different situations are summarized in Fig. 9 and means that for the smallest field sizes Eq. (2) strictly does no longer hold.

The constraint imposed by the lack of CPE, that is, when $\Phi_{\text{med}} \neq \Phi_{\text{det}}$, can be overcome using direct Monte Carlo calculations to compute an overall conversion factor to transfer D_{det} into D_{med} , which is achieved by computing the quantity (see e.g., ref. [53])

$$F_{\text{det},Q} = \frac{D_{\text{med},Q}(P)}{\bar{D}_{\text{det},Q}} \quad (3)$$

where $D_{\text{med},Q}(P)$ is the absorbed dose to the medium at a point P , usually simulated as a very small volume of water, and $\bar{D}_{\text{det},Q}$ is the averaged absorbed dose calculated inside the detector. It is obvious that for a situation where $\Phi_{\text{med}} \approx \Phi_{\text{det}}$, Eq. (3) reduces to

$$F_{\text{det},Q} = s_{\text{med,det}} p_{\text{ch},Q} \quad (4)$$

which are the quantities appearing in Eq. (2).

8 Fluence dependence on detector material and design

It has been seen so far that perturbation effects in small fields are caused by differences in electron fluence in the detector and in the otherwise homogeneous fluence in the medium, i.e. $\Phi_{\text{med}} \neq \Phi_{\text{det}}$, and that currently their value is determined using a Monte Carlo-calculated ratio $D_{\text{med}}/\bar{D}_{\text{det}}$. It is of interest at this stage to understand the differences in electron (and photon) fluence spectra inside small field detectors, how these compare with fluence spectra in a water medium, and how these differences relate with the absorbed dose inside a detector.

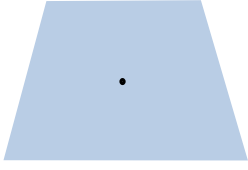
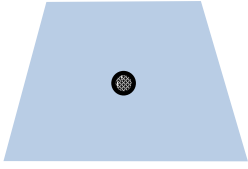
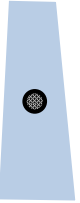
Beam type	Beam-detector configuration	Fluence in det & med	Bragg-Gray applicability
(a) Broad/large		$\Phi_{\text{det}} = \Phi_{\text{med}}$	Ideal detector (\equiv B-G), TCPE $D_{\text{med},Q}(P) = D_{\text{det},Q}(P) s_{\text{med,det}}$
(b) Broad/large		$\Phi_{\text{det}} \approx \Phi_{\text{med}}$	Real detector (\approx B-G), TCPE $D_{\text{med},Q}(P) = \bar{D}_{\text{det},Q} s_{\text{med,det}} \prod p_i$ small, approx. independent perturbations \Rightarrow corrected by p_i
(c) Narrow/small		$\Phi_{\text{det}} \neq \Phi_{\text{med}}$	Real detector (\neq B-G), no TCPE $D_{\text{med},Q}(P) \neq \bar{D}_{\text{det},Q} s_{\text{med,det}} \prod p_i$ large, non-indept. perturbations \Rightarrow B-G breaks-down Use MC: $F_{\text{det},Q} = \frac{D_{\text{med},Q}(P)}{\bar{D}_{\text{det},Q}}$
			(c) reduces to (b) if $\Phi_{\text{det}} \approx \Phi_{\text{med}}$, i.e. $F_{\text{det},Q} = s_{\text{med,det}} \prod p_i$

Figure 9: Applicability of cavity theory to different beam size and detector combinations: (a) corresponds to an ideal Bragg-Gray detector in a broad beam, where $\Phi_{\text{med}} = \Phi_{\text{det}}$; (b) represents a real detector in a broad beam, i.e. when $\Phi_{\text{med}} \approx \Phi_{\text{det}}$, and requires an electron fluence perturbation correction factor close to unity; (c) corresponds to a real detector in a beam that is insufficiently broad for the establishment of charged particle equilibrium; in this case the electron fluence in the detector is significantly different from that in the undisturbed medium, $\Phi_{\text{med}} \neq \Phi_{\text{det}}$, requiring a large perturbation correction factor, i.e. Bragg-Gray conditions have broken down. From Andreo *et al.* (2017) [52]. Copyright Wiley-VCH Verlag GmbH & Co KGaA. Reproduced with permission.

During the past few years it has commonly been assumed that the reasons for $\Phi_{\text{med}} \neq \Phi_{\text{det}}$ are largely due to the different mass density of the medium (water) and of the detector intrinsic material (air, silicon, diamond, etc.). This led to the proposal for a *density perturbation effect* to be included in the cavity theory for small photon fields (see, e.g., refs. [16, 19, 21, 33]). Recently, it has been argued that the reason for $\Phi_{\text{med}} \neq \Phi_{\text{det}}$, that is, for the response of a detector in small fields, is due to the mass stopping power of the radiation sensitive volume (RSV) of the detector relative to water and by the constructional details of the detector ([44, 45]). These two components make the fluence inside the detector to differ, sometimes substantially, from the fluence in the undisturbed medium (water), thereby violating the condition for charge-particle equilibrium and breaking down Bragg-Gray cavity theory.

8.1 Role of the detector material

Figure 10 shows ratios of mass electronic stopping powers of different materials to water as a function of electron energy, $[S_{\text{el}}(E)/\rho]_{\text{med,w}}$; some of these materials are commonly used as solid-state detectors. The *mass density* (ρ , in g cm^{-3}) and the *mean excitation energy* (the *I*-value, in eV) of each material are shown in the figure within parenthesis. It can be observed that the energy dependence of the stopping-power ratio of a detector RSV material-to-water depends strongly on the *I*-value and to a lesser extent on its *electron density* ($n_e \propto \rho Z/A$). At low electron energies the energy dependence of the stopping-power

ratio is governed solely by the I -value, and at energies above a few hundred keV by the combined effect of the I -value and the electron density n_e , both parameters entering into the so-called *density-effect* of the mass electronic stopping power, δ ; approximate energies of the onset of δ are indicated in Fig. 10. The dependence of the density-effect on n_e and the I -value can be understood from the approximate

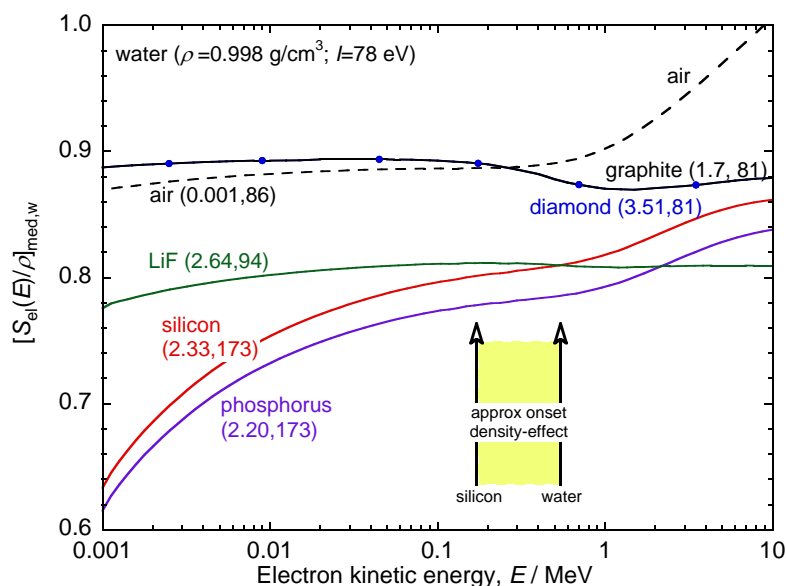


Figure 10: Ratios of mass electronic stopping powers med-to-water, $[S_{el}(E)/\rho]_{med,w}$, as a function of the electron energy, for different materials. The mass density (in g cm^{-3}) and mean excitation energy (I -value, in eV) of each material are given within parenthesis. Note the onset of the density-effect δ at energies of a few hundred keV. Adapted from Andreo and Benmakhrouf (2017) [44]. Copyright Institute of Physics and Engineering in Medicine. Reproduced by permission of IOP Publishing. All rights reserved.

expression for the mass electronic stopping power (c.f. refs. [44, 52])

$$\frac{1}{\rho} S_{el} \propto \frac{Z}{A} \frac{1}{\beta^2} \left[f(\beta) - \ln I - \delta(I^2, \rho \frac{Z}{A}, \beta) \right] \quad (5)$$

which does not include an explicit dependence on the mass density of the medium (similar, for instance, to that of photon mass attenuation or mass energy-absorption coefficients). In the equation, $f(\beta)$ is a function of the electron velocity in units of the speed of light in vacuum ($\beta = v/c$), and δ is the density-effect of the stopping power that in the expression shows its dependence on different fundamental quantities, where the squared value of the mean excitation energy (I^2) plays a dominant role.

For a 6 MV small photon beam the electron spectrum (fluence differential in energy, Φ_E) inside a small detector volume shows different trends depending on the energy region that we consider. At low electron energies, where the density-effect is practically negligible (below a few hundred keV), detector materials with a stopping power lower than that of water (due to their higher I -value) yield an electron fluence inside the detector which is higher than that in water (see Fig. 11(a)). This is clearly independent of the material mass density. It should be noted that low electron energies (approximately below 400 keV) account for up to 25% of the absorbed dose in the RSV of a silicon detector [44]. The trend gets blurred at high energies, as the differences in stopping-power ratios of the different materials in this energy region are relatively small. The differential absorbed dose (strictly, the *differential restricted cema*, $C_{\Delta,E}$, because there is no reason to assume CPE) can be calculated at each energy as the product $\Phi_E S_{el}(\Delta, E)/\rho dE$, where $S_{el}(\Delta, E)/\rho$ is the restricted stopping power with $\Delta = 10$ keV, which is shown in Fig. 11(b) for the different materials as an approximate “dose spectrum”. Here it can be seen

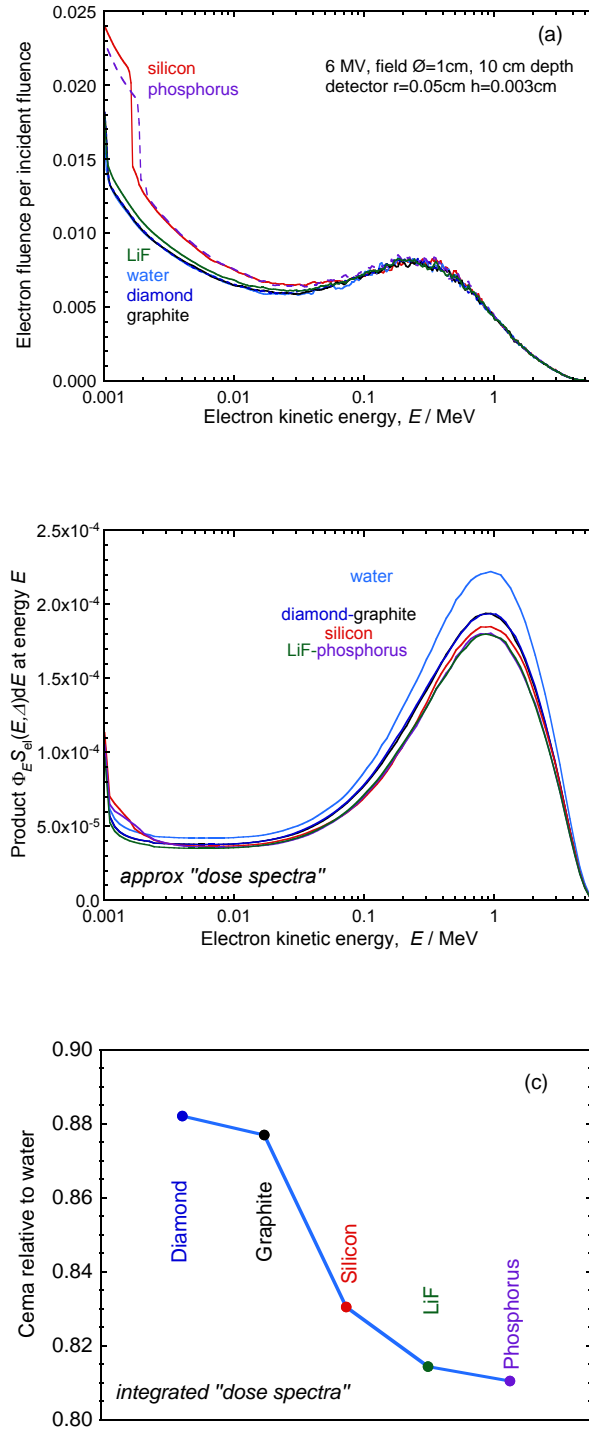


Figure 11: (a) Electron fluence differential in energy, per incident photon fluence, in small volumes of different detector materials inserted at 10 cm depth in a water phantom irradiated by a 6 MV narrow photon beam. (b) Differential restricted-cema values, given by $C_{\Delta,E} = \Phi_E S_{el}(\Delta, E)/\rho dE$, showing that the most probable value of $C_{\Delta,E}$ occurs at $E \approx 1$ MeV. (c) Integrated restricted cema values C_{Δ} relative to water; note that the order of the top-to-bottom sequence coincides with that of the $(S_{el}/\rho)_{med,w}$ -ratios at 1 MeV in Fig. 10. From Andreo and Benmakhlouf (2017) [44]. Copyright Institute of Physics and Engineering in Medicine. Reproduced by permission of IOP Publishing. All rights reserved.

that at the energy of the peak of the differential dose spectrum, approximately at 1 MeV, it is the stopping power of the different materials what governs its height. The integral of these spectra yields the total absorbed dose within each detector (strictly, the *restricted cema*, C_{Δ}), and can be observed in Fig. 11(c) that, relative to water, the magnitude of the different values follows the order of the stopping-power ratios at 1 MeV in Fig. 10, that is, the absorbed dose in the detector is governed by the combined effect of the I -value and the density effect δ , but not by the mass density ρ as a single parameter.

It should be emphasized that there is no contradiction in the results for square field sizes smaller than about 1 cm of, e.g., Scott *et al.* using 15 MV [16], and those of Andreo and Benmakhlouf using 6 MV [44], for silicon and diamond RSVs, even if the detector volumes were different, but on their interpretation. In both cases the result was $D_{\text{diam}} > D_{\text{Si}}$ (shown as $F_{\text{diam}} < F_{\text{Si}}$ in fig. 2 of ref. [16]), which is consistent with the results for other materials in Fig. 11c, showing that for these materials a lower I -value results in a higher absorbed dose. This was also verified in ref. [54], although for large 6 MV fields and in the context of radiotherapy treatment planning, comparing the absorbed dose in two water volumes having the same density but different I -values, and obtaining $D_{\text{w}}(\text{low } I) > D_{\text{w}}(\text{high } I)$, in consistency with $S_{\text{el,w}}/\rho(\text{low } I) > S_{\text{el,w}}/\rho(\text{high } I)$, and also in agreement with Fig. 11c. Additionally, ref. [44] used volumes scaled with the electron density of the detector material (the O'Connor scaling theorem [55]), obtaining the same trend for the dose vs. $(S_{\text{el}}/\rho)_{\text{med,w}}$ as for unscaled volumes.

Rather than using their silicon vs. diamond MC results, the conclusion of ref. [16] regarding the role of the detector mass density in small fields was based on the comparison of results for fictitious ‘water with diamond density’ and ‘water with silicon density’. The authors used the same atomic composition and mass electronic stopping power as for ordinary water, i.e., the only parameter changed was the mass density, and obtained the result $D_{\text{w}}(\text{diam}) > D_{\text{w}}(\text{Si})$. This procedure was biased due to two reasons. First, the authors did not compare two materials differing in anything else than their mass density, so that the influence of Z/A and the I -value could not be accounted for. Second, and against the authors’ procedure for using the same stopping powers for both ‘fictitious waters’, changing the water mass density while using the same atomic composition (and hence the same Z/A and I -value) does change the mass electronic stopping powers at energies above a few hundred keV, where the onset of the density-effect, δ , occurs. This can easily be demonstrated by comparing the mass electronic stopping powers of liquid water and water vapour using the same I -value, which will be identical below the onset of δ , but not above this threshold. (In reality, the I -value of water vapour is about 5 % lower than that of liquid water, resulting in a $(S_{\text{el}}/\rho)_{\text{vapour,liquid}} > 1$, from about 2 % at 1 keV to 1 % at the onset of δ , from where it increases progressively as does the air/water ratio in Fig. 10.)

These arguments lead to question the conclusion in ref. [16] regarding the role of the detector mass density. If instead of ‘fictitious water’ other materials differing in Z/A (small effect) and I -value (large effect) but with similar densities would have been used, the same conclusion as in refs. [44, 54] regarding the role of stopping-power ratios would have been obtained. It should also be mentioned that the ICRU-90 [56] recommendation for using the graphite crystallite density (2.265 g cm^{-3}) instead of the bulk density (e.g., 1.7 g cm^{-3}) should have been implemented for the diamond density-effect correction file, whereas the mass density of 3.5 g cm^{-3} should only be used for the Monte Carlo simulations. This remark, however, does not modify noticeably the results of ref. [16].

8.2 Influence of detector design

Let us now consider the photon and electron spectra at 10 cm depth produced by a 6 MV photon beam inside real detectors, calculated with Monte Carlo simulations of different detectors using detailed descriptions of their geometry provided by the respective manufacturers. They are compared with the spectra in a small volume of water for $10 \text{ cm} \times 10 \text{ cm}$ and $0.5 \text{ cm} \times 0.5 \text{ cm}$ field sizes.

Photon spectra are shown in Fig. 12 for (a) a natural diamond detector, (b, c) two unshielded silicon diode detectors from different manufacturers, and (d) a shielded silicon diode detector.

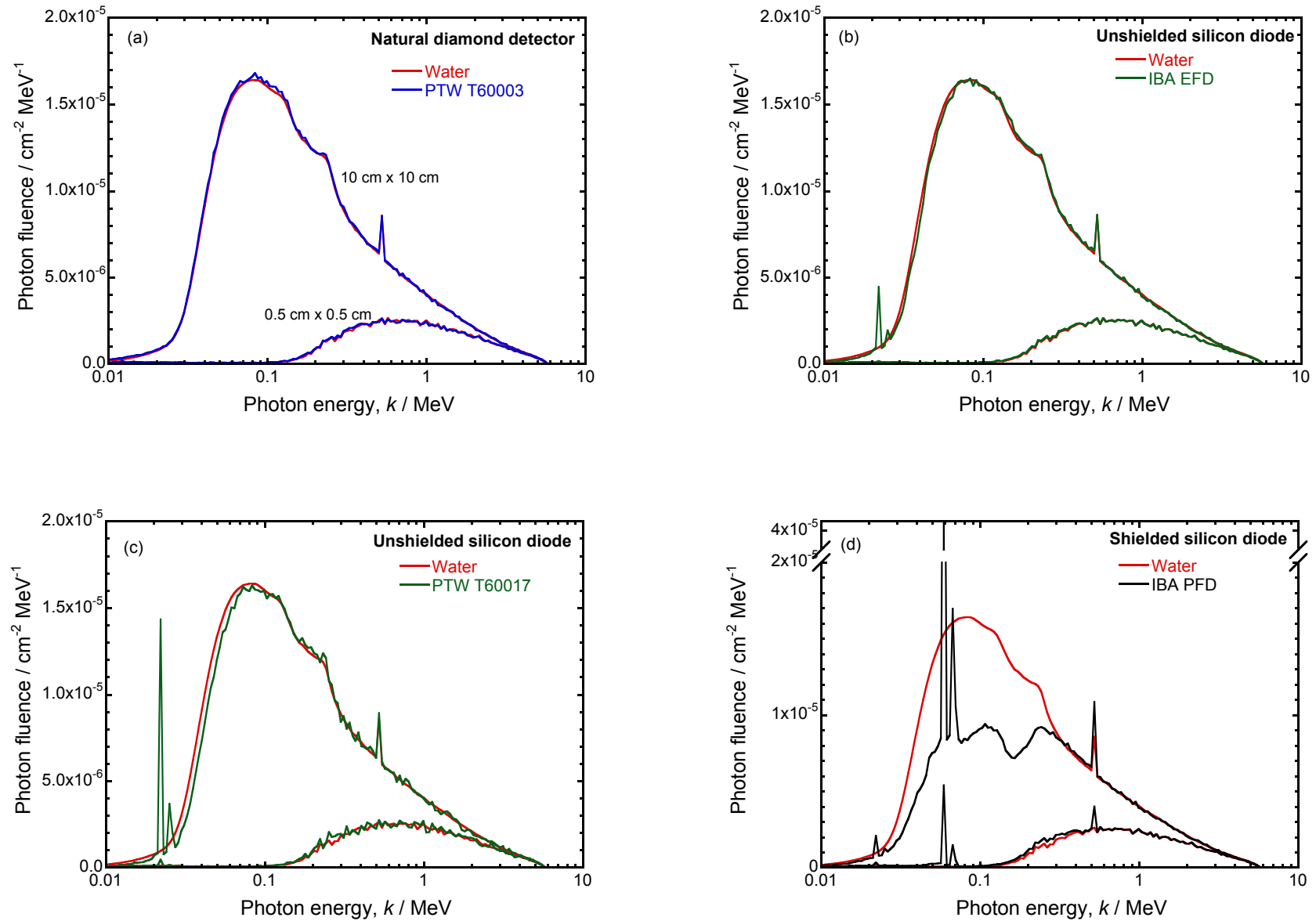


Figure 12: Monte Carlo calculated photon fluence spectra (Φ_k) as a function of the photon energy, scored in the radiation sensitive volume of different detectors at 10 cm depth, for 6 MV photon beams. The large spectra in each figure are for a $10 \text{ cm} \times 10 \text{ cm}$ field and the small spectra for $0.5 \text{ cm} \times 0.5 \text{ cm}$. From Benmakhlof and Andreo (2017) [45]. Copyright John Wiley & Sons Inc. Reproduced with permission.

In the figure it can be observed that:

- (i) For the two field sizes, the spectra in the diamond detector are practically identical to those in water. The substantial filtration of low-energy photons as a result of the decrease in field size is noticeable, as was also illustrated in Fig. 4. The positron annihilation peak at 511 keV shown in the 10 cm \times 10 cm field has been filtered in the small field size.
- (ii) For the two field sizes, the spectra for the two unshielded diodes are also very similar to those in water. They show, however, peaks at low energies that correspond to characteristic x rays generated in thin metallic layers surrounding the silicon volume, even if they are classified as “unshielded diodes”. The design of the two diodes is clearly different and from the energy of the x-ray peaks one could infer the materials used; in one of the diodes these materials yield a slight spectral difference with water, particularly for the 10 cm \times 10 cm field, which is unnoticeable for the other detector.
- (iii) For the shielded diode the substantial filtration of low-energy photons in the 10 cm \times 10 cm field can be observed, making the spectrum very different from that in water. This is the expected filtration in a broad beam, for which the shielding was designed, which will result in a very different fluence ratio between the large and the small field than in the unshielded detectors. The x-ray peaks of the shielding material show that the filtration of low-energy photons is less efficient than what one would expect. Note that due to these reasons, while shielded diodes are useful detectors for broad photon beams, they are not the best option for small field relative dosimetry.

Electron spectra, which are the final responsible for the energy absorbed in the detectors, are on the other hand strongly dependent on the detector material as one can infer from the previous discussion on stopping-power ratios (see Section 8.1). Figure 13 shows electron fluence distributions for a variety of detectors, which includes (a) three small ionization chambers, (b) two diamond detectors, and (c) unshielded and (d) shielded diodes (four and two types, respectively), where it can be seen that:

- (i) Despite the large difference in density between water and air, the spectra inside the three ionization chambers are relatively similar to those in water for the two field sizes.
- (ii) This is also the case, even more pronounced, for the two diamond detectors, which, in consistency with the discussion on stopping-power ratios above, shows that despite the high detector mass density, the spectra are quite similar to that in water.
- (iii) The spectra for the two types of silicon diodes, unshielded and shielded, do not differ substantially between each other, but are very different from the spectra in water, again justified in terms of the stopping-power ratio silicon-to-water and the very large difference in I -values for the two materials ($I_{\text{Si}}/I_{\text{w}} = 2.2$). The relatively small fluence discrepancy between shielded and unshielded diodes is originated by the shielding materials; they are smaller than what one would expect, but it should be recalled that unshielded diodes also include thin layers of high- Z materials surrounding the silicon RSV.

It is also of interest to compare the contribution to the electron fluence in the RSV material with that of the material surrounding the RSV for small field sizes. For that purpose, the fluence has been calculated inside an unshielded diode detector for a 0.5 cm \times 0.5 cm field size under different assumptions: (i) a detailed Monte Carlo simulation of the detector, as in Fig. 13(c); (ii) a simulation that assumes the RSV to be water; and (iii) a simulation that assumes that the high- Z material surrounding the water RSV of case (ii) has unit mass density.

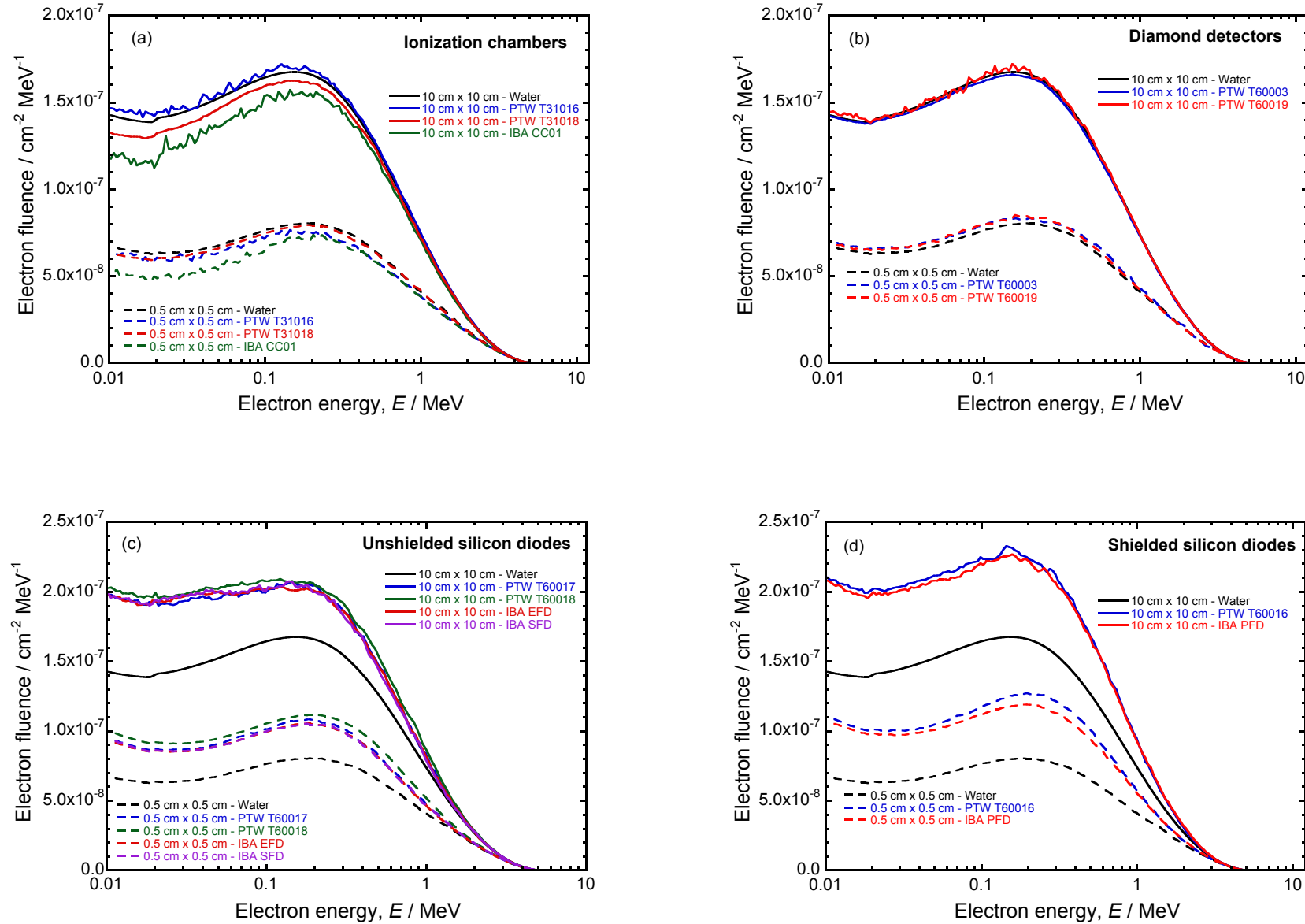


Figure 13: Monte Carlo calculated electron fluence spectra (Φ_E) as a function of the electron energy, scored in the radiation sensitive volume of different detectors at 10 cm depth, for 6 MV photon beams. The spectra represented by continuous lines in each figure are for a 10 cm x 10 cm field and the dashed lines for 0.5 cm x 0.5 cm. From Benmakhlof and Andreo (2017) [45]. Copyright John Wiley & Sons Inc. Reproduced with permission.

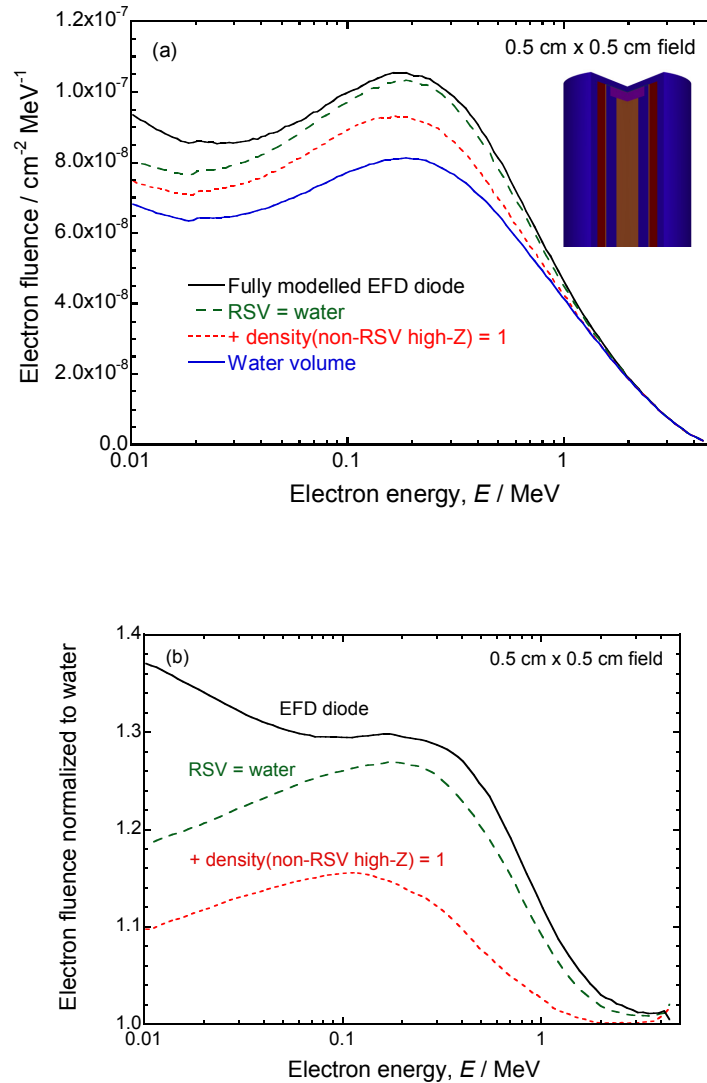


Figure 14: (a) Monte Carlo calculated electron fluence spectra (Φ_E) scored in a fully modelled IBA EFD diode (upper solid line), a fully modelled EFD with a RSV of water (dashed line), a fully modelled EFD with a RSV water and unit density for the high- Z non-RSV components (dotted line), and in a small volume of water (lower solid line). The spectra are for $0.5 \text{ cm} \times 0.5 \text{ cm}$, 6 MV photon beams. (b) Spectra normalized to the fluence in the small water volume. From Benmakhlouf and Andreo (2017) [45]. Copyright John Wiley & Sons Inc. Reproduced with permission.

Results are shown in Fig. 14, illustrating the Monte Carlo calculated spectra (a), and their values normalized to the spectra in water (b). Case (ii), with RSV=water, shows a large difference with the spectra in water and provides an estimate of the importance of the material surrounding the RSV (indicated by “non-RSV” in the figure), as under this assumption, the spectral difference does not depend on the intrinsic detector material. If the RSV is water and the surrounding high- Z material has unit density, case (iii), the fluence approaches that in water, resulting in about half of the difference that in case (ii). Note that the remaining difference with the spectra in water of case (iii) is due to the I -value of the high- Z material and its influence on the density effect, as only its mass density has been changed, and to the influence of other low- Z materials in the detector whose physical and atomic properties have not been modified in the Monte Carlo simulations.

In general, it can be concluded that, even for an unshielded diode, the influence of high- Z materials surrounding the detector RSV is larger than that due to the fluence difference between the intrinsic material of the detector RSV and water.

9 Field output factors for relative dosimetry

In principle, the relative dosimetry of small fields is quite similar to that of large fields, where the dose in a clinical field f_{clin} is related to the dose in the standard reference field f_{ref} (10 cm \times 10 cm) through the so-called *output factor*¹. It is defined as the ratio between the dose in the fields f_{clin} and f_{ref} at the reference depth z_{ref} .

For broad beams this ratio is normally approximated by the ratio of detector readings, that is

$$\text{OF}_{z_{\text{ref}}}(f_{\text{clin}}) = \frac{D(z_{\text{ref}}, f_{\text{clin}}, \text{SAD})}{D_{\text{ref}}(z_{\text{ref}}, 10 \times 10, \text{SAD})} \approx \frac{M(z_{\text{ref}}, f_{\text{clin}}, \text{SAD})}{M_{\text{ref}}(z_{\text{ref}}, 10 \times 10, \text{SAD})} \quad (6)$$

where SAD (source-to-axis distance) can be replaced by SSD (source-to-surface distance) depending on the technique being used (isocentric or constant SSD). The approximation is justified by the practical constancy with field size of stopping-power ratios and perturbation factors for large fields, for a given photon beam quality.

Recall that the new formalism for the reference dosimetry of small fields implemented in IAEA TRS-483, often cited as the *Alfonso formalism* [8], is based on the adoption of a *machine-specific reference field* (*msr field*), f_{msr} . For machines that cannot realize the standard reference field f_{ref} of 10 cm \times 10 cm, the *msr field* is taken to be the largest possible field in that generator, e.g., 6 cm diameter in a CyberKnife treatment unit, 5 cm \times 10 cm in a Tomotherapy machine, etc. A detector used to measure in these fields must extend at least a distance r_{LCPE} from the external detector boundary. For a conventional linac the *msr field* coincides with the standard reference field, i.e. $f_{\text{msr}} \equiv f_{\text{ref}} = 10 \text{ cm} \times 10 \text{ cm}$.

Note also that for composite beams like in IMRT, the Alfonso formalism also introduced the concept of *plan-class specific reference field* (*pcsr field*), f_{pcsr} , which is a reference radiation field made of a combination of multiple beams, in a configuration that is as close as possible to a final clinical delivery scheme. Although some proposals have been made for this concept (see e.g., refs.[59, 60, 61], the development of criteria for defining *pcsr* fields has, unfortunately, been rather scarce and for this reason no dosimetry recommendations have yet been produced.

For the relative dosimetry of small f_{clin} beams the approximation of Eq. (6) is, however, not applicable because, even if for a given beam quality stopping-power ratios are practically constant with field size, perturbation factors and volume averaging effects depend considerably on the detector type and size, on the field size and on the accelerator type (effective source size), as discussed in previous sections. It is then necessary to apply strictly the definition of output factor as a *dose ratio* in the two fields, which for a clinical field f_{clin} and the reference *msr* field f_{msr} is written as

$$\Omega_{Q_{\text{clin}}, Q_{\text{msr}}}^{f_{\text{clin}}, f_{\text{msr}}} = \frac{D_{w, Q_{\text{clin}}}^{f_{\text{clin}}}}{D_{w, Q_{\text{msr}}}^{f_{\text{msr}}}} = \frac{M_{Q_{\text{clin}}}^{f_{\text{clin}}}}{M_{Q_{\text{msr}}}^{f_{\text{msr}}}} k_{Q_{\text{clin}}, Q_{\text{msr}}}^{f_{\text{clin}}, f_{\text{msr}}} \quad (7)$$

where, to avoid confusion with other symbols commonly used for broad beams, the symbols $\Omega_{Q_{\text{clin}}, Q_{\text{msr}}}^{f_{\text{clin}}, f_{\text{msr}}}$ (or $\Omega_{Q_{\text{clin}}, Q_{\text{ref}}}^{f_{\text{clin}}, f_{\text{ref}}}$), with the fields and beam qualities written explicitly, is used in the Alfonso formalism [8] and in IAEA TRS-483 [7]; Ω is called the *field output factor*. Note that the dose ratio in the middle term of Eq. (7) is replaced by the rightmost hand-side term that includes the ratio of detector readings, i.e. the same as in Eq. (6), but multiplied by a factor $k_{Q_{\text{clin}}, Q_{\text{msr}}}^{f_{\text{clin}}, f_{\text{msr}}}$. This multiplier is called *field output correction factor*, and converts the detector readings ratio into a true dose ratio.

The field output correction factor $k_{Q_{\text{clin}}, Q_{\text{msr}}}^{f_{\text{clin}}, f_{\text{msr}}}$ is determined using Monte Carlo simulations or experimental comparisons with the response of an “ideal” detector taken as reference. Both methods have

¹Note that there is no consensus on the term adopted for this factor, which in the literature is referred to as *output factor*, *relative dose factor*, or *total scatter factor* (see e.g., refs. [57, 58, 6], respectively).

advantages and disadvantages:

- The Monte Carlo method can simulate very accurately any detector-field size-linac configuration, but assumes that all detectors of a given model and make are identical. Ignoring detector-to-detector differences, particularly for small ionization chambers or solid-state detectors, is often a rather optimistic approach that can only be compensated by an increase in the uncertainty estimation (e.g., a type B uncertainty) of the field output correction factor. In addition, the geometry description provided by manufacturers might not be accurate enough (c.f. refs. [30, 41, 42]) and the potential influence of the electric field around the detector RSV, which may affect its response, is ignored.
- An experimental determination depends not only on the precision (repeatability and reproducibility) of the measurements, but is also based on the use of a detector that is assumed to be practically ‘ideal’, that is, the necessary corrections are well known, or its response is not affected by perturbations or constraints of any kind, or by special conditions of use. The latter refers to the potentially complicated methodology for measuring with some detectors; for example, liquid ionization chambers show high recombination effects that require considerable corrections for saturation, the response of certain diamond detectors shows a strong dose rate dependence, etc.

Some detectors can be considered to be highly suitable for relative dosimetry, as EBT radiochromic films, for which ICRU-91 [3] indicates the disadvantages of requiring an elaborated measuring protocol, non-linear response and limited reproducibility for low doses. Other detectors are claimed to be ‘ideal’, mostly by their developers. This is the case, for instance, with (a) plastic scintillator fibres (see, e.g., refs. [62, 63]), for which ICRU-91 points the constraints of Cerenkov correction and LET dependence, (b) some silicon arrays (see, e.g., ref. [64]), always subject to the constraints discussed in previous sections for silicon, to which energy dependence and perturbations, as well as a likely ageing effect, can be added, and (c) MOSFET detectors (see, e.g., ref. [65]), for which ICRU-91 indicates the constraints of energy dependence and perturbations caused by the substrate. The latter two types are designed for quality control measurements, but developers praise their performance for measuring field output factors. Only unbiased research, as opposed to developers or manufacturer claims, will demonstrate their true advantages and disadvantages in the near future. An overall review of chemical and solid state detectors can be found in ref. [52].

Data from IAEA TRS-483 [7] for the $k_{Q_{\text{clin}}, Q_{\text{ref}}}^{f_{\text{clin}}, f_{\text{ref}}}$ correction factors of multiple detector types, with $f_{\text{ref}} \equiv f_{\text{msr}}$, are shown in Fig. 15, where the large range of values obtained for different detector types, especially for the smallest field sizes, can be observed. These values were obtained from the statistical analysis of the results given in a large number of publications providing Monte Carlo-calculated and experimental data. From the figure it can be seen that for the smallest field sizes some detectors require a considerable field output correction factor, well above the usual maximum recommended $\pm 5\%$ for any type of correction (see e.g., ref. [7]). In addition, a suitable detector in small beams can become unsuitable in medium or larger beams, or the reverse. An example of the former is the unshielded diode for the smallest field size, and for the latter a Farmer-type ionization chamber. The most prudent approach is to perform measurements in small beams with different detector types, using the appropriate $k_{Q_{\text{clin}}, Q_{\text{ref}}}^{f_{\text{clin}}, f_{\text{ref}}}$ correction, and assign their mean value to the field output factor $\Omega_{Q_{\text{clin}}, Q_{\text{ref}}}^{f_{\text{clin}}, f_{\text{ref}}}$. Obtaining consistency in the determination of field output factors with different detector types is probably the best approach to ensure accuracy in the dosimetry of small beams.

10 Conclusions

This review shows that the physics of small megavoltage photon beam dosimetry can be rather complex. There are, in general, more aspects and important issues to consider than for conventional broad beams.

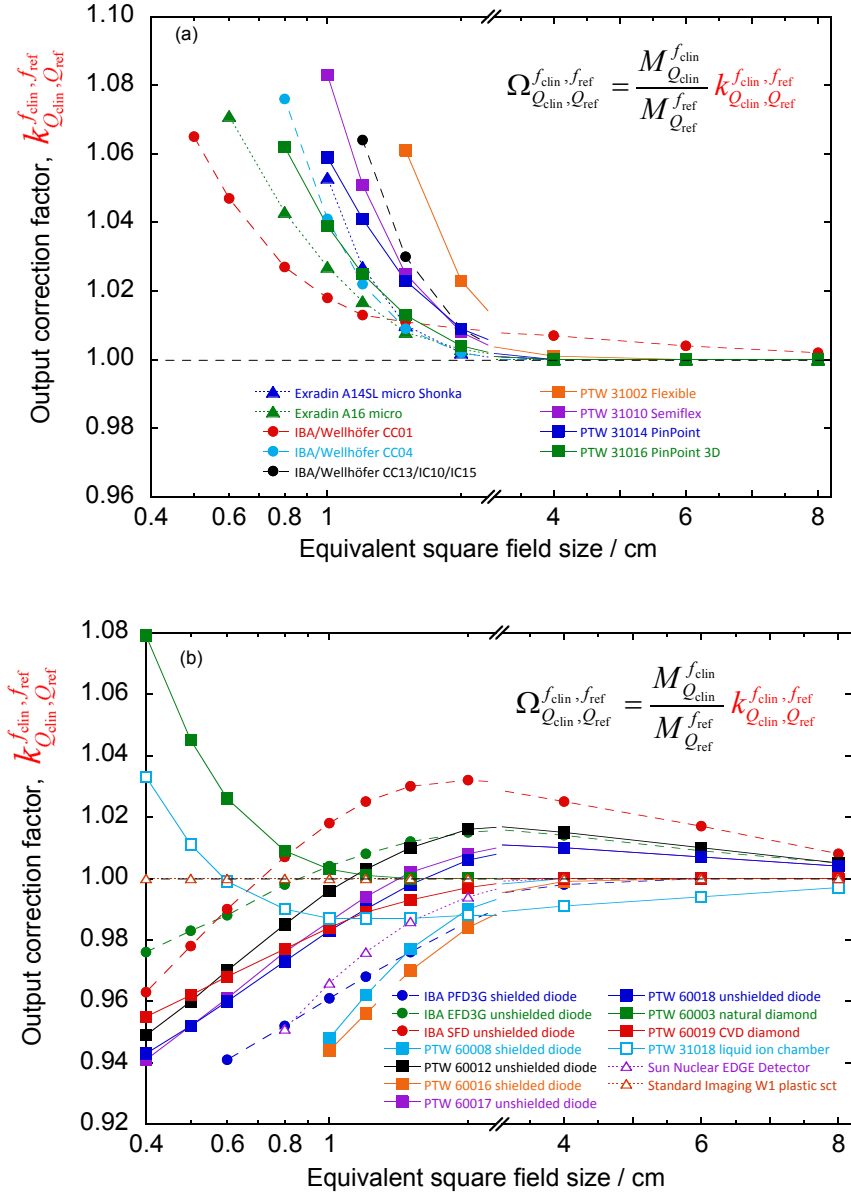


Figure 15: Field output correction factors $k_{Q_{clin}, Q_{ref}}^{f_{clin}, f_{ref}}$ for different detector types in 6 MV linac beams: (a) small ionization chambers; (b) solid-state and other detectors. Note the logarithmic scale in the abscissa axis below about 2.5 cm field size. Data from IAEA TRS-483 [7].

Perturbation and anomalous effects induced by a number of influence parameters, like detector perturbation factors and volume averaging, depend considerably on the detector material and its design, on the field size relative to the detector size, and on the accelerator type (effective source size). These may have a significant impact on reference dosimetry, to the extent of breaking down Bragg-Gray theory and, strictly, invalidate the use of common expressions based on the existence of charged-particle equilibrium.

The adequacy of the so far assumed role of a detector mass density to interpret the detector response and postulate a ‘density perturbation factor’ is questioned on the grounds of the $\rho Z/A$ and I -value dependence of the density-effect correction and mass electronic stopping powers. It is argued that detector response should be described in terms of stopping-power ratios detector-to-water, mainly due to the different I -values and to a lesser extent to the different electron densities ($n_e \propto \rho Z/A$). Using instead a ‘material perturbation factor’ would fully take into account the differences in atomic composition ($\rho Z/A$ and I -value) that govern stopping-power ratios.

Although relative dosimetry is conceptually simple, perturbation effects impact considerably the values of field output factors for different detector types, which cannot be assumed to be given by a ratio of detector readings. The influence of detector design can be significant, as is the case with some silicon diodes. Comparisons between different detector types provide valuable information on their adequacy for small field dosimetry.

Acknowledgements

Parts of the material in this review have been developed in collaboration with the members of the IAEA-AAPM Working Group* on “Small and Non-standard Field Dosimetry”. Special thanks are due to the core-authors of the IAEA-AAPM TRS-483 Code of Practice (underlined below).

* R. Alfonso, P. Andreo, R. Capote, K. Christaki, S. Huq, J. Izewska, J. Johansson, W. Kilby, T. R. Mackie, A. Meghzifene, H. Palmans (chair), J. Seuntjens and W. Ullrich

References

- [1] L Leksell. The stereotaxic method and radiosurgery of the brain. *Acta Chir. Scand.*, 102:316–319, 1951.
- [2] L Leksell. Cerebral radiosurgery. i. gammathalanotomy in two cases of intractable pain. *Acta Chir. Scand.*, 134:585–595, 1968.
- [3] ICRU. *Prescribing, Recording and Reporting of Stereotactic Treatments with Small Photon Beams*. ICRU Report 91. International Commission on Radiation Units and Measurements, Bethesda, MD, 2017.
- [4] W. Bogdanich and R. R. Ruiz. Radiation errors reported in Missouri, The New York Times (New York Edition), p. A17, 25 February 2010.
- [5] S. Derreumaux, G. Boisserie, G. Brunet, I. Buchheit, and T. Sarrazin. Concerns in France about the dose delivered to the patients in stereotactic radiation therapy. In *Standards, Applications and Quality Assurance in Medical Radiation Dosimetry (Proc. Int. Symp. Vienna)*, volume 1, pages 273–286. IAEA, Vienna, 2011.
- [6] M. M. Aspradakis, J. P. Byrne, H. Palmans, J. Conway, K. Rosser, A. P. Warrington, and S. Duane. *Small field MV photon dosimetry*. IPEM Report 103. Institute of Physics and Engineering in Medicine, York, UK, 2010.
- [7] H. Palmans, P. Andreo, K. Christaki, M. S. Huq, and J. Seuntjens. *Dosimetry of small static fields used in external beam radiotherapy: An IAEA-AAPM international Code of Practice for reference and relative dose determination*. IAEA Technical Report Series No. 483. International Atomic Energy Agency, Vienna, 2017.
- [8] R. Alfonso, P. Andreo, R. Capote, M. S. Huq, W. Kilby, P. Kjall, T. R. Mackie, H. Palmans, K. Rosser, J. Seuntjens, W. Ullrich, and S. Vatnitsky. A new formalism for reference dosimetry of small and nonstandard fields. *Med. Phys.*, 35:5179–5186, 2008.
- [9] I. J. Das, G. X. Ding, and A. Ahnesjö. Small fields: Non-equilibrium radiation dosimetry. *Med. Phys.*, 35:206–215, 2008.
- [10] F. Crop, N. Reynaert, G. Pittomvils, L. Paelinck, C. De Wagter, L. Vakaet, and H. Thierens. The influence of small field sizes, penumbra, spot size and measurement depth on perturbation factors for microionization chambers. *Phys. Med. Biol.*, 54:2951–2969, 2009.
- [11] G. Cranmer-Sargison, S. Weston, J. A. Evans, N. P. Sidhu, and D. I. Thwaites. Implementing a newly proposed Monte Carlo based small field dosimetry formalism for a comprehensive set of diode detectors. *Med Phys*, 38:6592–6602, 2011.
- [12] P. Francescon, S. Cora, and N. Satariano. Calculation of $k_{Q_{\text{clin}}, Q_{\text{msr}}}^{f_{\text{clin}}, f_{\text{msr}}}$ for several small detectors and for two linear accelerators using Monte Carlo simulations. *Med. Phys.*, 38:6513–6527, 2011.
- [13] G. Cranmer-Sargison, S. Weston, J. A. Evans, N. P. Sidhu, and D. I. Thwaites. Monte Carlo modelling of diode detectors for small field MV photon dosimetry: detector model simplification and the sensitivity of correction factors to source parameterization. *Phys Med Biol*, 57:5141–5153, 2012.
- [14] E. Pantelis, A. Moutsatsos, K. Zourari, L. Petkokokinos, L. Sakelliou, W. Kilby, C. Antypas, P. Papagiannis, P. Karaikos, E. Georgiou, and I. Seimenis. On the output factor measurements of the CyberKnife iris collimator small fields: Experimental determination of the $k_{Q_{\text{clin}}, Q_{\text{msr}}}^{f_{\text{clin}}, f_{\text{msr}}}$ correction factors for microchamber and diode detectors. *Med Phys*, 39:4875–4885, 2012.
- [15] A. Ralston, P. Liu, K. Warrener, D. McKenzie, and N. Suchowerska. Small field diode correction factors derived using an air core fibre optic scintillation dosimeter and EBT2 film. *Phys Med Biol*, 57:2587–2602, 2012.
- [16] A. J. D. Scott, S. Kumar, A. E. Nahum, and J. D. Fenwick. Characterizing the influence of detector density on dosimeter response in non-equilibrium small photon fields. *Phys. Med. Biol.*, 57:4461–4476, 2012.
- [17] C. Bassinet, C. Huet, S. Derreumaux, G. Brunet, M. Chéa, M. Baumann, T. Lacornerie, S. Gaudaire-Josset, F. Trompier, P. Roch, G. Boisserie, and I. Clairand. Small fields output factors measurements and correction factors determination for several detectors for a CyberKnife and linear accelerators equipped with microMLC and circular cones. *Med Phys.*, 40:071725, 2013. Erratum: *Med. Phys.* 40:117201, 2013.

- [18] W. Lechner, H. Palmans, L. Sölkner, P. Grochowska, and D. Georg. Detector comparison for small field output factor measurements in flattening filter free photon beams. *Radioth. Oncol.*, 109:356–360, 2013.
- [19] J. D. Fenwick, S. Kumar, A. J. Scott, and A. E. Nahum. Using cavity theory to describe the dependence on detector density of dosimeter response in non-equilibrium small fields. *Phys Med Biol*, 58:2901–2923, 2013.
- [20] D. Czarnecki and K. Zink. Monte Carlo calculated correction factors for diodes and ion chambers in small photon fields. *Phys Med Biol*, 58:2431–2444, 2013. Corrigendum: *Phys. Med. Biol.* 59:791–794, 2014.
- [21] T. S. Underwood, H. C. Winter, M. A. Hill, and J. D. Fenwick. Detector density and small field dosimetry: integral versus point dose measurement schemes. *Med Phys*, 40:082102, 2013.
- [22] J. U. Wuerfel. Dose measurements in small fields. *Med. Phys. Int.*, 1:81–90, 2013.
- [23] G. Azangwe, P. Grochowska, D. Georg, J. Izewska, J. Hopfgartner, W. Lechner, C. E. Andersen, A. Beierholm, J. Helt-Hansen, H. Mizuno, A. Fukumura, K. Yajima, C. Gouldstone, P. Sharpe, A. Meghzifene, and H. Palmans. Detector to detector corrections: a comprehensive experimental study of detector specific correction factors for beam output measurements for small radiotherapy beams. *Med. Phys.*, 41:072103, 2014.
- [24] H. Benmakhlouf, J. Sempau, and P. Andreo. Output correction factors for nine small field detectors in 6 MV radiation therapy photon beams: a PENELOPE Monte Carlo study. *Med Phys*, 41:041711, 2014.
- [25] P. Francescon, S. Beddar, N. Satariano, and I. J. Das. Variation of $k_{Q_{\text{clin}}, Q_{\text{msr}}}^{f_{\text{clin}}, f_{\text{msr}}}$ for the small-field dosimetric parameters percentage depth dose, tissue-maximum ratio, and off-axis ratio. *Med. Phys.*, 41:101708, 2014.
- [26] C. Moignier, C. Huet, and L. Makovicka. Determination of the $k_{Q_{\text{clin}}, Q_{\text{msr}}}^{f_{\text{clin}}, f_{\text{msr}}}$ correction factors for detectors used with an 800 MU/min CyberKnife system equipped with fixed collimators and a study of detector response to small photon beams using a Monte Carlo method. *Med Phys*, 41:071702, 2014.
- [27] J. E. Morales, S. B. Crowe, R. Hill, N. Freeman, and J. V. Trapp. Dosimetry of cone-defined stereotactic radiosurgery fields with a commercial synthetic diamond detector. *Med Phys*, 41:111702, 2014.
- [28] P. Papaconstadopoulos, F. Tessier, and J. Seuntjens. On the correction, perturbation and modification of small field detectors in relative dosimetry. *Phys Med Biol*, 59:5937–5952, 2014.
- [29] A. Ralston, M. Tyler, P. Liu, D. McKenzie, and N. Suchowerska. Over-response of synthetic microdiamond detectors in small radiation fields. *Phys. Med. Biol.*, 59:5873–5881, 2014.
- [30] P. Andreo, H. Palmans, M. Marteinsdottir, H. Benmakhlouf, and Å. Carlson-Tedgren. On the Monte Carlo simulation of small-field micro-diamond detectors for megavoltage photon dosimetry. *Phys Med Biol*, 61:L1–L10, 2015.
- [31] H. Benmakhlouf, J. Johansson, I. Paddick, and P. Andreo. Monte Carlo calculated and experimentally determined output correction factors for small field detectors in Leksell Gamma Knife Perfexion beams. *Phys Med Biol*, 60:3959–3973, 2015.
- [32] H. Benmakhlouf. *Key Data for the Reference and Relative Dosimetry of Radiotherapy and Diagnostic and Interventional Radiology Beams*. PhD thesis, Stockholm University, 2015. <https://www.diva-portal.org/smash/get/diva2:792325/FULLTEXT03.pdf>.
- [33] H. Bouchard, J. Seuntjens, S. Duane, Y. Kamio, and H. Palmans. Detector dose response in megavoltage small photon beams. I. Theoretical concepts. *Med Phys*, 42:6033, 2015.
- [34] H. Bouchard, Y. Kamio, H. Palmans, J. Seuntjens, and S. Duane. Detector dose response in small megavoltage photon beams. II. Pencil beam perturbation effects. *Med. Phys.*, 42:6048–6061, 2015.
- [35] A. González-López, J. A. Vera-Sánchez, and J. D. Lago-Martín. Small fields measurements with radiochromic films. *J Med Phys*, 40:61–67, 2015.
- [36] S. Kumar, J. D. Fenwick, T. S. Underwood, D. D. Deshpande, A. J. Scott, and A. E. Nahum. Breakdown of Bragg-Gray behaviour for low-density detectors under electronic disequilibrium conditions in small megavoltage photon fields. *Phys Med Biol*, 60:8187–8212, 2015.

- [37] J. M. Lárraga-Gutierrez, P. Ballesteros-Zebadúa, M. Rodríguez-Ponce, O. A. García-Garduño, and O. O. Galván de la Cruz. Properties of a commercial PTW-60019 synthetic diamond detector for the dosimetry of small radiotherapy beams. *Phys. Med. Biol.*, 60:905–924, 2015.
- [38] N. Ploquin, G. Kertzscher, E. Vandervoort, J. E. Cygler, C. E. Andersen, and P. Francescon. Use of novel fibre-coupled radioluminescence and RADPOS dosimetry systems for total scatter factor measurements in small fields. *Phys Med Biol*, 60:1–14, 2015.
- [39] S. Tanny, N. Sperling, and E. I. Parsai. Correction factor measurements for multiple detectors used in small field dosimetry on the Varian Edge radiosurgery system. *Med Phys*, 42:5370, 2015.
- [40] T. S. Underwood, B. C. Rowland, R. Ferrand, and L. Vieilleveigne. Application of the Exradin W1 scintillator to determine Ediode 60017 and microDiamond 60019 correction factors for relative dosimetry within small MV and FFF fields. *Phys Med Biol*, 60:6669–6683, 2015.
- [41] P. Andreo and H. Palmans. Comment on “Experimental determination of the PTW 60019 microDiamond dosimeter active area and volume”. *Med. Phys.*, 43:6667, 2016.
- [42] M Marinelli, G. Prestopino, C. Vernoia, and G. Verona-Rinati. Experimental determination of the PTW 60019 microDiamond dosimeter active area and volume”. *Med. Phys.*, 43:5205–5212, 2016.
- [43] D. J. O’Brien, L. Leon-Vintro, and B. McClean. Small field detector correction factors $k_{Q_{clin}, Q_{msr}}^{f_{clin}, f_{msr}}$ for silicon-diode and diamond detectors with circular 6 MV fields derived using both empirical and numerical methods. *Med Phys*, 43:411, 2016.
- [44] P. Andreo and H. Benmakhlouf. Role of the density, density effect and mean excitation energy in solid-state detectors for small photon fields. *Phys. Med. Biol.*, 62:1518–1532, 2017.
- [45] H. Benmakhlouf and P. Andreo. Spectral distribution of particle fluence in small field detectors and its implication on small field dosimetry. *Med. Phys.*, 44:713–724, 2017.
- [46] X. A. Li, M. Soubra, J. Szanto, and L. H. Gerig. Lateral electron equilibrium and electron contamination in measurements of head-scatter factors using miniphantoms and brass caps. *Med. Phys.*, 22:1167–1170, 1995.
- [47] P. Papaconstadopoulos. *On the detector response and the reconstruction of the source intensity distribution in small photon fields*. PhD thesis, PID: 141364. McGill University, Montreal, 2016. http://digitool.Library.McGill.CA:80/R/-?func=dbin-jump-full&object_id=141364&silolibrary=GEN01.
- [48] F. Sánchez-Doblado, P. Andreo, R. Capote, A. Leal, M. Perucha, R. Arráns, L. Núñez, E. Mainegra, J. I. Lagares, and E. Carrasco. Ionization chamber dosimetry of small photon fields: a Monte Carlo study on stopping-power ratios for radiosurgery and IMRT beams. *Phys. Med. Biol.*, 48:2081–2099, 2003.
- [49] P. Andreo and A. Brahme. Stopping power data for high-energy photon beams. *Phys. Med. Biol.*, 31:839–858, 1986.
- [50] K. Eklund and A. Ahnesjö. Fast modeling of spectra and stopping-power ratios using differentiated fluence pencil kernels. *Phys. Med. Biol.*, 53:4231–4247, 2008.
- [51] T Kawachi, H Saitoh, M Inoue, T Katayose, A Myojoyama, and K Hatano. Reference dosimetry condition and beam quality correction factor for cyberknife beam. *Med. Phys.*, 35:4591–4598, 2008.
- [52] P. Andreo, D. T. Burns, A. E. Nahum, J. Seuntjens, and F. H. Attix. *Fundamentals of Ionizing Radiation Dosimetry*. Wiley-VCH, Weinheim, Germany, 2017.
- [53] J. Sempau, P. Andreo, J. Aldana, J. Mazurier, and F. Salvat. Electron beam quality correction factors for plane-parallel ionization chambers: Monte Carlo calculations using the PENELOPE system. *Phys. Med. Biol.*, 49:4427–4444, 2004.
- [54] P. Andreo. Dose to ‘water-like’ media or dose to tissue in mv photons radiotherapy treatment planning: still a matter of debate. *Phys. Med. Biol.*, 60:309–337. Corrigendum in p. 2619, 2015.

- [55] J. E. O'Connor. The variation of scattered x-rays with density in an irradiated body. *Phys. Med. Biol.*, 1:352–369, 1957.
- [56] ICRU. *Key Data for Ionizing Radiation Dosimetry: Measurement Standards and Applications*. ICRU Report 90. International Commission on Radiation Units and Measurements, Bethesda, MD, 2016.
- [57] E. G. A. Aird, J. E. Burns, M. J. Day, S. Duane, T. J. Jordan, A. Kacperek, S. C. Klevenhagen, R. M. Harrison, S. C. Lillicrap, A. L. McKenzie, W. G. Pitchford, J. E. Shaw, and C. W. Smith. *Central Axis Depth Dose Data for Use in Radiotherapy*. Brit. J. Radiol. Suppl. 25. The British Institute of Radiology, London, 1996.
- [58] E. B. Podgorsak. External photon beams: Physical aspects. In E. B. Podgorsak, editor, *Radiation Oncology Physics: a Handbook for Teachers and Students*, pages 161–217. International Atomic Energy Agency, Vienna, 2005.
- [59] K. E. Rosser and J. L. Bedford. Application of a new dosimetry formalism to volumetric modulated arc therapy (VMAT). *Phys Med Biol*, 54:7045–7061, 2009.
- [60] T. Öhrman, P. Andreo, U. Isacsson, and A. Montelius. Analytical determination of a plan class specific reference (pcsr) field for reference dosimetry of IMRT fields. Book of Extended Synopsis, IAEA International Symposium. In *Standards, Applications and Quality Assurance in Medical Radiation Dosimetry*, pages 319–320, Vienna, 2010. Vienna: International Atomic Energy Agency.
- [61] A Gago-Arias, R Rodríguez-Romero, P Sánchez-Rubio, D M González-Castaño, F Gómez, L Núñez, H Palmans, P Sharpe, and J Pardo-Montero. Correction factors for A1SL ionization chamber dosimetry in Tomotherapy: machine-specific, plan-class, and clinical fields. *Med. Phys.*, 39:1964–1970, 2012.
- [62] A. S. Beddar and T. M. Briere. Plastic scintillation detectors. In D. W. O. Rogers and J. E. Cygler, editors, *Clinical Dosimetry Measurements in Radiotherapy*, pages 1059–1082. Medical Physics Publishing, Madison, WI, 2009.
- [63] A. S. Beddar and L. Beaulieu. *Scintillation Dosimetry*. CRC Press-VitalSource Bookshelf Online, Boca Raton, FL, 2016.
- [64] K Al Shukaili, M Petasecca, M Newall, A Espinoza, V L Perevertaylo, S Corde, M Michael Lerch, and A B Rosenfeld. A 2D silicon detector array for quality assurance in small field dosimetry: DUO. *Med. Phys.*, 44:628–636, 2017.
- [65] W Loong Jong, N Min Ung, A Vannyat, Z Jamalludin, A Rosenfeld, and J Hsiu Ding Wong. “Edge-on” MOSkin detector for stereotactic beam measurement and verification. *Physica Medica*, 33:127–135, 2017.